ACS APPLIED MATERIALS & INTERFACES
Research Article
www.acsami.org

Effect of Electrode Materials on AlN-Based Bipolar and Complementary Resistive Switching

Chao Chen, Shuang Gao, Guangsheng Tang, Huadong Fu, Guangyue Wang, Cheng Song, Fei Zeng,* and Feng Pan*

Laboratory of Advanced Materials, Department of Materials Science and Engineering, Tsinghua University, Beijing 100084, People's Republic of China

Supporting Information

ABSTRACT: We report the complementary resistive switching (CRS) behaviors in aluminum nitride (AlN)-based memory devices as the promising new material system for large-scale integration of passive crossbar arrays. By utilizing different electrodes (Cu, Pt, and TiN), CRS characteristics are demonstrated in both TiN/AlN/Cu/AlN/TiN electrochemical metallization cells and Pt/AlN/TiN/AlN/Pt ionic resistive switching systems. The instability of Pt/AlN/Cu/AlN/Pt based CRS is explained by the relatively small reset voltage caused by the thermal effects enhanced reset process in the corresponding bipolar resistive switching element. It is concluded that the prerequisite for reliable and stable CRS is that the reset voltage of the bipolar resistive switching element must be much larger than half of the set voltage.

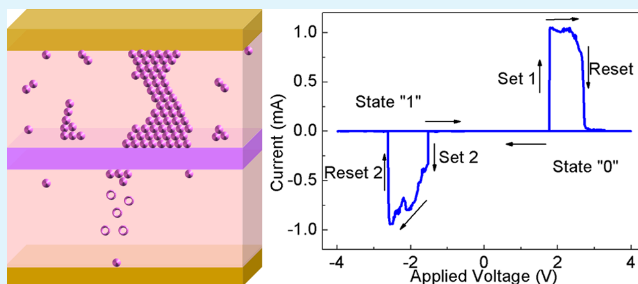

KEYWORDS: *complementary resistive switching, AlN, bipolar resistive switching, filament, memristor, RRAM*

INTRODUCTION

Resistive random access memory (RRAM) has been becoming increasingly attractive and important for the promising candidate for next-generation nonvolatile memory, because of its fast operation speed, low power consumption, and excellent scalability in passive crossbar arrays by producing the ultimately cell size in theory,[1−5] i.e., $4F^2$, where F is the minimum feature size. The integration density can be further increased to $4F^2/n$ by 3-dimentional stacking n layers of crossbar.[6] However, because of the so-called sneak current problem, the read of a specific memory cell in the passive crossbar array is highly susceptible. The sneak current is caused by the parasitic current flowing through neighboring ON-state cells in the crossbar network. Various rectifying devices, such as Schottky diode and nonlinear selectors at each cross-point, have been explored to solve the sneak current problem.[5,7−11] Much effort has been dedicated to the integration of the RRAM crossbar arrays and the selection devices. But it is still a challenging issue to obtain the scalable selection devices with sufficient reverse/forward resistance ratio and high forward current density.[12] Recently, Waser and co-workers proposed the concept of complementary resistive switches (CRS) to solve the sneak current problem by connecting two bipolar resistive switches (BRS) antiserially.[13,14] Subsequently, Lee et al. demonstrated a successful working crossbar device in 30 nm scale Ta_2O_{5-x}/TaO_{2-x} bilayer structure.[15] Although the CRS device needs a complicated and destructive read operation as well as tricky fabrication processes, it has attracted extensive and significant research interest.[16−21] Because of the unnecessary use of external selection devices, CRS device is one of the considerable candidates for suppressing sneak current. Further development of the CRS devices such as extended voltage readout window and enhanced on/off ratio would promote the industrialization of the high-density RRAM crossbar arrays.

Aluminum nitride (AlN), known as an important wide band gap semiconductor, has been demonstrated to exhibit attractive resistive switching behavior.[22−26] AlN possesses many excellent features for RRAM applications, including high thermal conductivity, good insulating properties and high dielectric constant, which could result in superior switching performance of AlN-based RRAM.[22,27] Thus, it would be of great interest and significance to develop the nitride-based CRS device. The nitride-based CRS device can avoid the formation of an instable interface during the device fabrication compared to oxide films.[22,23] Furthermore, some metallic nitrides, such as TiN, TaN, and WN, are widely used in semiconductor industry as electrode materials. This makes the semiconducting nitride a potentially outstanding CRS material for passive crossbar arrays applications.

Here we present the CRS behavior in magnetron sputtering deposited AlN-based structures with different electrode materials, e.g., Cu, Pt, and TiN. Reliable and stable CRS characteristics were successfully demonstrated in both TiN/AlN/Cu/AlN/TiN electrochemical metallization cells and Pt/

Received: December 15, 2012
Accepted: February 5, 2013
Published: February 20, 2013

ACS Publications © 2013 American Chemical Society

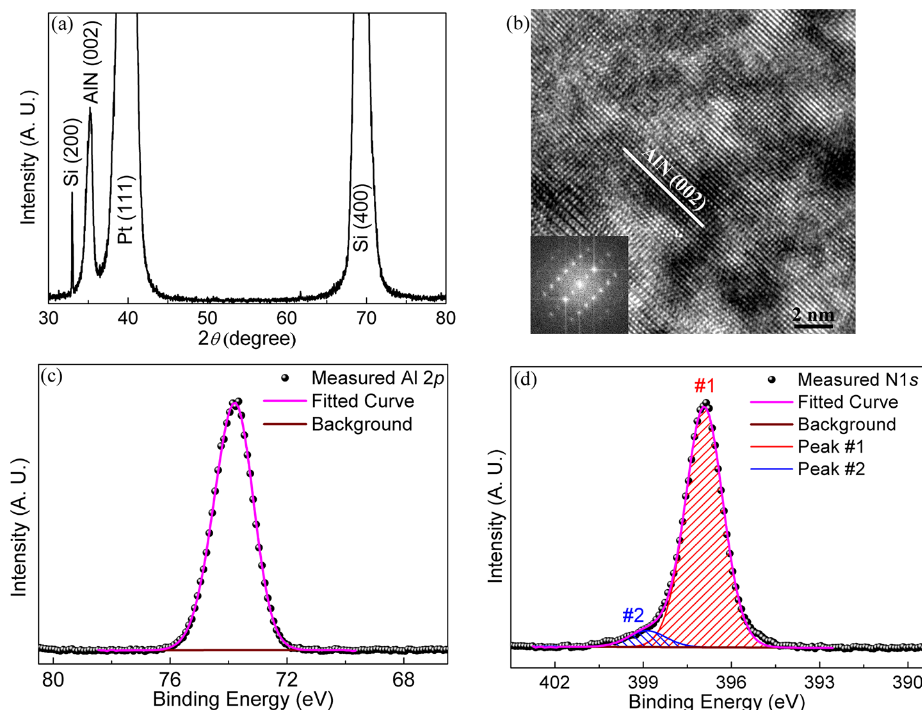

Figure 1. (a) XRD patterns of AlN film deposited on Pt/Ti/SiO_2/Si substrates. (b) Cross-sectional high-resolution TEM image of AlN film. The inset is the corresponding fast Fourier transform (FFT). (c) Al 2p and (d) N 1s XPS spectra of as-deposited AlN film. The solid sphere is the measured data and the magenta line is the fitting result.

AlN/TiN/AlN/Pt ionic resistive switching systems. The influences of thermal effects enhanced reset process and electrochemical redox reaction mediated reset process on the stable CRS behavior are discussed.

EXPERIMENTAL DETAILS

Materials. In this work, AlN films were deposited by means of direct current (DC) reactive magnetron sputtering method, using an aluminum target (99.99% purity, 3 in. in diameter). The base vacuum of the chamber was better than 5×10^{-5} Pa and the sputtering pressure was fixed at 0.4 Pa, which was made up of a mixture of 0.25 Pa argon (99.95% purity) and 0.15 Pa nitrogen (99.95% purity). During the deposition process, temperature of the substrate was held at 300 °C. TiN films were fabricated also by the DC reactive magnetron sputtering with a titanium target (99.99% purity, 3 in. in diameter). The sputtering conditions for TiN films are almost the same as that used in AlN films deposition (0.4 Pa working gas mixed of 0.25 Pa argon and 0.15 Pa nitrogen, 300 °C). The Cu and Pt electrodes are deposited by a simple DC magnetron sputtering (argon: 0.4 Pa) at room temperature (RT).

Device Fabrication and Characterization. Two types of device are fabricated in this work. Sandwiched electrode/AlN/electrode device are delivered for BRS measurement, while penta-layer memory device, e.g. Pt/AlN/Cu/AlN/Pt, TiN/AlN/Cu/AlN/TiN, and Pt/AlN/TiN/AlN/Pt, are created for achieving the CRS behavior. Circular top electrodes (TE) with diameter of 100 μm are deposited with the aid of a shadow mask, defining the lateral geometry of the devices. The thicknesses of TE, AlN film and bottom electrode (BE) used in these memory devices are approximately 120, 50, and 120 nm, respectively, while the intermediate electrode of 40 nm is employed in CRS devices, as can be seen from the scanning electron microscopy (SEM) image in Figure S1 in the Supporting Information. For electrical characterization, all DC (sweep speed of 5 V/s) measurements were performed using an Agilent B1500A semiconductor device analyzer at RT under air condition by applying voltage to the TE while the BE was grounded. The crystal structure of AlN films was examined in $\theta-2\theta$ mode by X-ray diffraction (XRD, Rigaku D/max-2500) utilizing Cu K_α radiation (λ = 0.15418 nm), whereas cross-sectional morphology was observed by field-emission SEM (LEO1530) and transmission electron microscopy (TEM, JEM-2010F). The chemical states were characterized by X-ray photoelectron spectroscopy (XPS, Kratos AXIS Ultra) after 2 min Ar^+(2 keV) etching of the specimen in order to avoid the possible influence of absorbed contaminations.

RESULTS AND DISCUSSION

The XRD spectra of the as-deposited AlN films grown on Pt/Ti/SiO_2/Si(100) substrates are shown in Figure 1a. Apart from (002) peak, no additional diffraction lines of AlN could be detected in the scanned range of 30−80°, indicating the hexagonal wurtzite crystal structure of the polycrystalline AlN film with a *c*-axis texture. AlN films grown on other substrates at the same condition also show the (002) texture, but the degree of texture is different (Figure S2 in the Supporting Information). TEM observations have also been performed to characterize the structures of AlN film. Figure 1b exhibits a cross-sectional high-resolution TEM (HRTEM) image of the AlN film, which indicates the high quality of crystallization of the AlN deposited at 300 °C.

Chemical states of Al and N elements in the AlN films were characterized by XPS. Figures 1c and 1d represent the XPS spectra of Al 2p and N 1s signals, respectively. The solid sphere trace reveals the measured spectra, while the magenta line is the fitted curve following Shirley background subtraction. As can be seen in Figure 1c, the Al 2p spectrum is sharp and symmetric with the main peak located at 73.7 eV, which can be well-fitted by single peak Gaussian curve with full width at half-maximum (fwhm) of 1.57 eV. No peak corresponding to metallic Al or Al−O bond was observed, indicating the aluminum bound to nitrogen in wurtzite AlN.[28,29] The N 1s spectrum is less symmetric with a shoulder on the high binding energy side. Deconvolution of the N 1s spectrum exhibits two subpeaks, as shown in Figure 1d. The main peak #1 centered at 396.9 eV

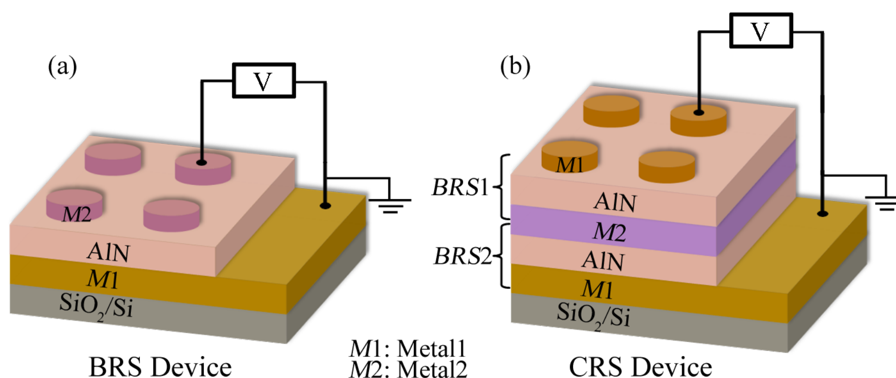

Figure 2. Schematic configurations of the AlN-based (a) BRS and (b) CRS devices and the measurement setup, where *M*1 and *M*2 denote two different metal electrodes. CRS device is composed of two BRS elements.

with fwhm of 1.5 eV corresponds to nitrogen bound to aluminum in wurtzite AlN.[28,29] The broad and low intensity peak #2 at 398.9 eV could be attributed to impurities such as N−C bond or the nitrogen bound present at grain boundaries.[29]

The schematic configurations of our two-terminal devices are depicted in Figure 2, where *M*1 and *M*2 denote the two different electrodes. Here, we regard Cu, Pt, and TiN electrodes used in this work all as metals. For BRS device, the AlN film is sandwiched by two different electrodes (*M*1 and *M*2) and all the bias voltages are applied between *M*1 and *M*2, as can be seen in Figure 2a. For CRS device, 5 layers of film are deposited sequentially on the SiO_2/Si substrate, which can be considered as connecting two BRS elements antiserially (BRS1 and BRS2). Electric fields are applied across the penta-layer CRS device, as shown in Figure 2b.

CRS, the promising building block for high density crossbar RRAM, manifests unique *I*−*V* curves and readout operations. Typically, the as-fabricated CRS device is in an insulating state which is only presented in the initial state, since the two antiserially connected BRS elements are in high resistance state (HRS) at first. An electro-forming process is needed to activate the CRS device and switch the device to a certain logic state ("1" or "0"). Figure 3 shows a sketch map of the typical *I*−*V* curves of CRS memory device and the corresponding logic storage state. For example, the logic "1" state of CRS device means that the upper BRS element of the CRS is in low resistance state (LRS) while the lower BRS element is in HRS,

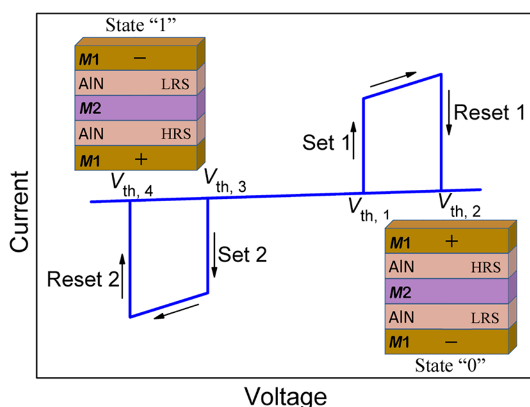

Figure 3. Sketch map of the representative *I*−*V* curves of CRS memory device and the corresponding logic storage states (top-left inset for state "1" and bottom-right inset for state "0").

as shown in the top-left inset of Figure 3. State "0" of CRS corresponds to the reversed configuration of the two BRS elements (bottom-right inset of Figure 3). If the CRS device is in state "1", almost all the voltage drops over the lower BRS element and the whole device manifests high resistance under low bias voltage. Until the voltage reaches $V_{th,\,1}$, the current increases abruptly, and both the upper and lower BRS elements are switched to LRS (Set 1 in Figure 3). This CRS state can be defined as the "ON" state which is commonly presented in the read operation. As the applied voltage is increased further till $V_{th,\,2}$ is reached, the current is declined again (Reset 1 in Figure 3), and the whole CRS device is switched to state "0". When negative voltage is applied, the CRS device is switched to "ON" state at $V_{th,\,3}$ and turns to state "1" at $V_{th,\,4}$. In order to detect the logic state of the CRS device, a voltage comes into the range between $V_{th,\,1}$ and $V_{th,\,2}$ is applied as the read operation. The readout window is defined as $V_{window} = V_{th,2} - V_{th,1}$. Whether state "1" or "0" is stored, one of the two BRS elements is in the HRS. Thus, the device always manifests high resistances at bias voltage lower than $V_{th,\,1}$, which enables CRS to avoid the sneak current problem in crossbar arrays structure.

To develop the AlN-based CRS memory device, trilayer BRS device and penta-layer CRS structures are fabricated and delivered to current−voltage (*I*−*V*) measurement. Altogether, we studied BRS behavior in Cu/AlN/Pt, Cu/AlN/TiN, and TiN/AlN/Pt memory devices. Likewise, the corresponding penta-layer structures as Pt/AlN/Cu/AlN/Pt, TiN/AlN/Cu/AlN/TiN, and Pt/AlN/TiN/AlN/Pt were investigated for CRS memory applications. Figure 4 shows the *I*−*V* curves of Cu/AlN/TiN device and the penta-layer CRS device. Bipolar switching behaviors are demonstrated, as can be seen in Figure 4a. The resistance of the device increased abruptly at about 1.5 V (Set) and returned to HRS at approximately −1.9 V with multistep reset process, yielding a HRS/LRS ratio of more than 1×10^3 at 0.2 V. A current compliance (CC) of 1 mA was adopted here in the set process in order to prevent the device from over current. The BRS characteristics of the Cu/AlN/TiN memory device are stable and reliable (see Figure S3 in the Supporting Information). Meanwhile, the penta-layer TiN/AlN/Cu/AlN/TiN structure exhibits steady CRS characteristics. When voltage was applied on the top TiN electrode, the TiN/AlN/Cu/AlN/TiN device was switched to the stable "ON" state at 1.7 V (−1.5 V) and turned back to the storage state at 2.7 V (−2.7 V), as shown in Figure 4b. The voltage and resistance readout windows of the device are about 1 V and 10^2, respectively. In addition, the CRS behavior can be consecutively

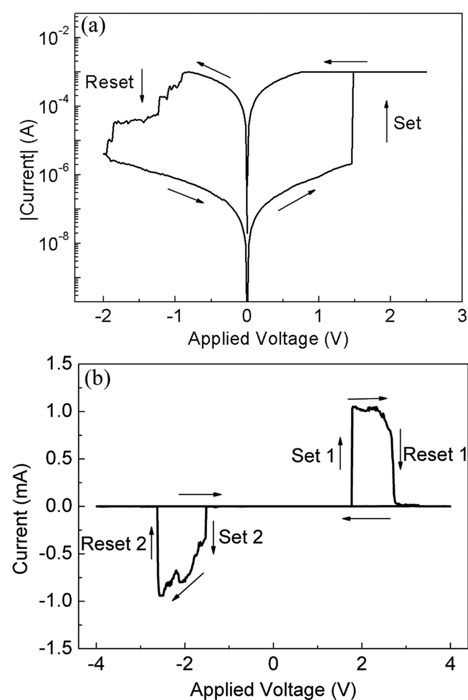

Figure 4. $I-V$ curves of (a) Cu/AlN/TiN BRS device and (b) TiN/AlN/Cu/AlN/TiN CRS device.

reproduced (see Figure S4 in the Supporting Information), which demonstrates the reliability of the CRS characteristics in the TiN/AlN/Cu/AlN/TiN device.

Figure 5a exhibits the $I-V$ curve of the Cu/AlN/Pt BRS device. To avoid the influence of CC on the resistive switching characteristics, the same value of CC as 1 mA was also adopted in the Cu/AlN/Pt device. The device switched from HRS to LRS at about 2.2 V (Set) and turned back to HRS at about −0.8 V (Reset) with HRS/LRS ratio of 1×10^5 at −0.2 V. The

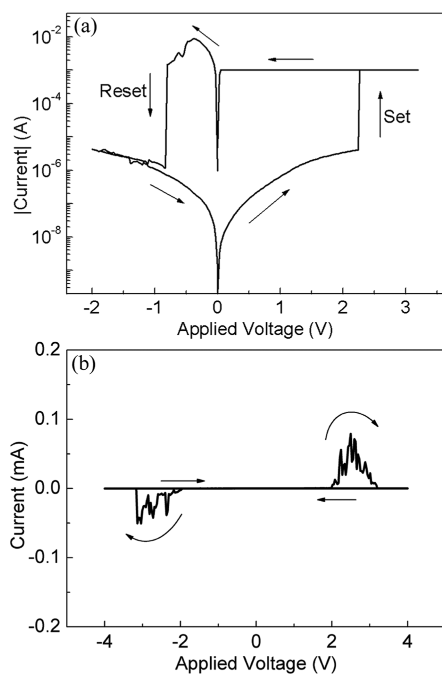

Figure 5. $I-V$ curves of (a) Cu/AlN/Pt BRS device and (b) Pt/AlN/Cu/AlN/Pt penta-layer structure.

BRS behavior in Cu/AlN/Pt device is also stable and reproducible, as can be seen in Figure S3 in the Supporting Information and our previous reports.[22] However, the $I-V$ curve of Pt/AlN/Cu/AlN/Pt structure is quite unstable, comparing with the TiN/AlN/Cu/AlN/TiN structure. As the voltage was swept in a sequence of 0 V→ 4 V→ −4 V→ 0 V, the structure exhibited a high resistance at small voltage. Then, a current turbulence happened at approximately 2 V, but the resistance of the structure did not reach a steady "ON" state. The current became fluctuant and decreased subsequently. The negative voltage on the device also results in the unstable current fluctuation, as shown in Figure 5b.

Generally, the Cu/AlN/TiN and Cu/AlN/Pt devices both belong to the electrochemical metallization cells. The resistive switching behavior of these systems is dominated by the electrochemical redox process in the storage medium and can be well-understood by the metal filament model.[3,30−32] As reported previously, Cu atoms are easily oxidized and reduced in a great number of semiconductors and insulators.[3,22,31,33] The Pt and TiN act as the electrochemically inert electrodes, whereas the Cu is the electrochemically active electrode that can be oxidized and reduced as[3,22]

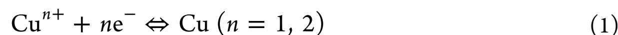

$$Cu^{n+} + ne^- \Leftrightarrow Cu \; (n = 1, 2) \quad (1)$$

Oxidation occurs on Cu electrodes under positive voltage and the Cu cations are generated and migrate to the inert counter electrode. This redox process results in the electrodeposit of Cu filaments which are preferentially formed through grain boundaries or any other crystal defects in AlN film. The rupture and reconnection of the Cu filament induce the HRS and LRS of the device, respectively.

In the TiN/AlN/Cu/AlN/TiN device here, the stable CRS processes can be explained by the different configuration of the Cu filaments in double AlN films, as schematically shown in Figure 6. If the device is in state "1", Cu filaments have been formed in the top AlN film whereas the bottom BRS element is in HRS. When a positive voltage is applied to the top TiN electrode, all the voltage drop across over the bottom AlN film and the Cu atoms at the middle Cu layer are oxidized (Figure 6a). Then, Cu^{n+} ions migrate toward the bottom TiN electrode, leading to the formation of Cu filaments in the bottom AlN film. Thus, the whole device is switched to the "ON" state (Figure 6b). Once Cu filaments are formed in both top and bottom AlN films, the two BRS elements have an equal voltage drop. With further increase in the applied voltage, the Cu filaments in the top AlN film begin to dissolve. After the top Cu filaments are ruptured, the whole device is switched to state "0". If negative voltage is applied to the bottom TiN electrode, the reverse process happens. Cu filaments are formed again in top AlN film (Set 2 in Figure 4), while the Cu filaments in bottom AlN film are dissolved. The whole device is switched back to state "1". Obviously, in this CRS device, state "0" or "1" is stored by the different internal configurations of Cu metal filaments. Since both states "0" and "1" exhibit high resistance at low voltage, the device can eliminate the sneak current in crossbar arrays.

Interestingly, although the Cu/AlN/Pt device shows stable BRS behaviors with large HRS/LRS ratio, the antiserially connection of the two devices only results in the unstable current switch. At the same time, the Cu/AlN/TiN device and the corresponding pentalayer structure manifest stable BRS and CRS characteristics, respectively. It is not difficult to understand

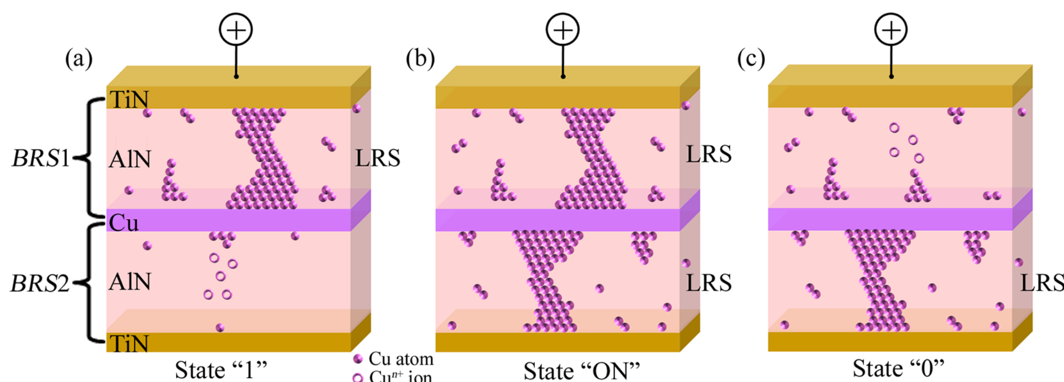

Figure 6. Schematic diagram for the mechanism of CRS effects in TiN/AlN/Cu/AlN/TiN electrochemical system. (a) State "1" of the device. Cu filament is formed in the top BRS element with bottom BRS element in HRS. (b) Intermediate state "ON". Cu filaments are formed in both BRS elements. (c) State "0" of the device. The Cu filament in top BRS element is ruptured while a Cu filament in bottom BRS element is recovered.

the differentiation of these two kinds of device if the threshold voltages of the CRS process are taken into considered.

Whenever the CRS device is in state "0" or "1", all the voltage drops over the BRS element with high resistance when voltage is applied to the device. Thus, the threshold voltages $V_{th,1}$ and $V_{th,3}$, which turns the CRS device to "ON" state are equal to the set voltage (V_{set}) in single BRS device. Once the CRS device is switched to "ON" state, both BRS elements have an equal voltage drop. We can calculate

$$|V_{th,1}| = |V_{th,3}| = |V_{set}| \tag{2}$$

$$|V_{th,2}| = |V_{th,4}| = 2|V_{reset}| \tag{3}$$

with V_{reset} as the reset voltage in single BRS device. To construct a stable CRS device, the readout window $V_{window} = V_{th,2} - V_{th,1}$ must be greater than zero. Combining formulas 2 and 3, we can obtain that the prerequisite for stable CRS is

$$|V_{reset}| > \frac{|V_{set}|}{2} \tag{4}$$

For Cu/AlN/Pt device, V_{set} is often twice higher than the V_{reset}, as shown in Figure 5a and the previous work,[22] whereas the threshold voltage of Cu/AlN/TiN device meets the requirement of formula 4. Thus, antiserially connection of two Cu/AlN/TiN elements builds a reliable and stable CRS device.

The different value of V_{reset} between Cu/AlN/Pt and Cu/AlN/TiN device implies the different mechanism in the resistance switching process, especially in the reset process. It is considered that the dissolution of metal filaments is mostly caused by the redox reaction under appropriate voltages.[3] On the other hand, the effects of Joule heating (I^2R, where I is the current, and R is the resistance) could not to be ignored, which can strongly enhance the redox process, even fuse the metal filament.[34−36] As shown in Figure 5a, the reset process of Cu/AlN/Pt device is relatively steeper than that of the Cu/AlN/TiN device. The resistance has increased by more than 1×10^3 times. Reset current (I_{reset}) as large as 9 mA is observed under CC of 1 mA. However, the reset process of Cu/AlN/TiN device exhibits stepwise switching and the maximum current is less than 1 mA under the same value of CC (Figure 4a). The power ($I \times V$) in the reset process of Cu/AlN/Pt device is rapidly raised to about 3.5 mW at 0.48 V, whereas the power of Cu/AlN/TiN device increase slowly to 0.8 mW at 0.88 V (see Figure S5 in the Supporting Information). Cumulative thermal effects in Cu/AlN/Pt device are much severer than that in Cu/AlN/TiN device. Thus, it is considered that thermal effects induced by Joule heating play an important role in the reset process of Cu/AlN/Pt device,[34,37] whereas electrochemically redox reaction dominates the reset process of Cu/AlN/TiN device.[3] Of course, thermal effects also contribute to the reset process in the Cu/AlN/TiN device but not that important in Cu/AlN/Pt device. Serious thermal effects lead to the small value of V_{reset}, while redox reaction results in the relatively large value of V_{reset}. The different reset species could originate from the different size of the Cu metal filament. As the AlN film grown on TiN film is not identical to that deposited on Pt film, the Cu filament in Cu/AlN/Pt device tends to be much stronger than that in Cu/AlN/TiN device when switched to LRS. The strong Cu metal filament in Cu/AlN/Pt device produces the large reset current, substantial Joule heating effects and small value of V_{reset}. The V_{reset} is much smaller than half of the V_{set} in Cu/AlN/Pt device, which does not reach the demand of formula 4. Consequently, the formation of Cu filament in one BRS element of the Pt/AlN/Cu/AlN/Pt CRS device would immediately cause the dissolution of Cu filament in the opposite BRS element. In the same way, the dissolution of Cu filament in one BRS device would depress the growth of Cu filament in the opposite BRS element. The current in the Pt/AlN/Cu/AlN/Pt CRS is not as high as that in Cu/AlN/Pt device (Figure 5b), which is just caused by the simultaneous growth and dissolution of Cu filament in the different BRS element of Pt/AlN/Cu/AlN/Pt CRS device. Hence, the CRS device could not reach the stable "ON" state. Undesired reset process always happens in one BRS element before the desired set in the other elements for Pt/AlN/Cu/AlN/Pt structure, whereas the TiN/AlN/Cu/AlN/TiN device shows stable CRS behavior.

Besides the electrochemical metallization system in which AlN film acts as the electrolyte materials, ionic resistive switching can be demonstrated in AlN-based systems.[24,26] In the TiN/AlN/Pt device, both Pt and TiN electrodes are electrochemically inert electrode and no metal cations are injected to the AlN film. This AlN-based ionic species also show stable BRS and CRS characteristics, as can be seen in Figure 7. Due to the intrinsically insulating feature of AlN, however, the ionic switching is more difficult to happen than the Cu-migration related electrochemical metallization. An electroforming process of large voltage is often required to activate the ionic switching effects in the system (see Figure S6 in the Supporting Information). After electroforming process,

dx.doi.org/10.1021/am303128h | ACS Appl. Mater. Interfaces 2013, 5, 1793−1799

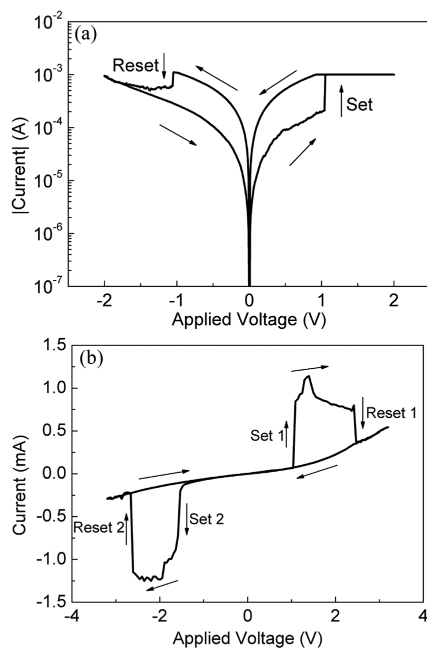

Figure 7. $I-V$ curves of (a) TiN/AlN/Pt BRS device and (b) Pt/AlN/TiN/AlN/Pt CRS device.

the TiN/AlN/Pt device shows antisymmetrical $I-V$ curve of resistive switching with reliability (see Figure S3 in the Supporting Information). Under the same CC of 1 mA, the device possesses nearly equivalent value of set and reset voltage (1 and −1 V) and small HRS/LRS ratio (less than 10). The corresponding penta-layer Pt/AlN/TiN/AlN/Pt structure also needs a two-step electroforming process before the resistive switching goes into action (see Figure S6 in the Supporting Information). After both the top and bottom AlN storage media are activated, the CRS behaviors are realized. The resistive switching phenomena of the penta-layer Pt/AlN/TiN/AlN/Pt structure are presented in Figure 7b, in which the intermediate "ON" state can be preserved during the switching process from one logic state to another with voltage readout window of more than 1 V and resistance readout windows of merely several times. The CRS behavior is reproducible (see Figure S4 in the Supporting Information), but shows poor endurance performance of only tens of DC sweep cycles. Owing to the variant crystallinity and composition of the AlN films grown on different substrates, the resistive switching characteristics such as threshold voltages and resistances of the two BRS elements in CRS device are nonuniform. Careful modulating of the fabrication processes is necessary to improve the endurance and reduce the device variations.

Apparently, the mechanism of CRS in this Pt/AlN/TiN/AlN/Pt device is not the same as the Cu metallic filament model in TiN/AlN/Cu/AlN/TiN device, because no external metal cations migrate into the AlN film.[24,38] The switching is proposed to be mediated by the filaments composed of defects.[24,26,36,39,40] The electroforming process could cause the active N-poor region of the AlN film responsible for resistive switching. Based on the consideration of the XPS results in Figure 1d, defects such as intrinsic nitrogen vacancies (V_N^+) or extrinsic carbon substitutional impurities (C_{Al}^+) could be the mobile ionic species and form the conductive filaments.[24,41] The precipitation and dissolution of the V_N^+ composed filaments induce the high and low resistance of the BRS device. The reversed configuration of the defects composed leakage filaments in AlN film lead to the different logic states of the Pt/AlN/TiN/AlN/Pt CRS device, which actually resembles the Cu metal filaments based system. Because of the nearly identical absolute value of set and reset voltage which is in accordance with the requirement of formula 4, the V_N^+ composed conductive filaments can be stabilized at both BRS elements of the Pt/AlN/TiN/AlN/Pt device in the voltage range between $V_{th,\,1}$ ($V_{th,\,3}$) and $V_{th,\,2}$ ($V_{th,\,4}$). At the same time, this ionic resistive switching based device possesses a relative small HRS/LRS ratio as to the metal filament system, which is regarded to be influenced by the high-voltage electroforming process and is not beneficial to the nonvolatile memory applications. Even the resistance readout window of TiN/AlN/Cu/AlN/TiN (1×10^2) is still inadequate for the stable reading and writing operation in large scale crossbar arrays.[12] Furthermore, the endurance of the present AlN-based CRS devices is still unsatisfactory and the device variations need continual improvement. The elimination of electroforming in BRS device and enlargement of both voltage and resistance readout window in AlN-based CRS systems are the crucial issues need to be addressed in the following studies. Further work includes fabricating the AlN-based CRS devices in actual crossbar arrays and manipulating the CRS by pulse, which are both in progress.

■ CONCLUSION

In summary, AlN-based CRS devices were fabricated using magnetron sputtering with a variety of electrode materials. The deposited AlN film were confirmed to be hexagonal wurtzite crystal structure with (002) preferential orientation. Reliable and stable CRS characteristics were successfully demonstrated in both TiN/AlN/Cu/AlN/TiN electrochemical metallization cells and Pt/AlN/TiN/AlN/Pt ionic resistive switching systems. However, the Pt/AlN/Cu/AlN/Pt structure shows unstable resistive switching, which is attributed to the small V_{reset} (less than half of V_{set}) in the Cu/AlN/Pt element. Thermal effects enhanced reset process, which induced by the large reset current flow through the filaments, cause the relatively small V_{reset}. More optimizations of the device performance, e.g., increase the readout window and depress the dispersity of threshold voltage, are necessary for the practical applications of AlN-based crossbar memory arrays.

■ ASSOCIATED CONTENT

Supporting Information

Further experimental details, SEM image of the CRS device, XRD patterns of AlN film deposited on different substrates, endurance and retention of the BRS devices, repeated CRS curves, power in the reset process and the electroforming process of the BRS and CRS devices. This material is available free of charge via the Internet at http://pubs.acs.org.

■ AUTHOR INFORMATION

Corresponding Author

*Tel.: +86-10-62772907. E-mail: panf@mail.tsinghua.edu.cn (F.P.); zengfei@mail.tsinghua.edu.cn (F.Z.)

Author Contributions

C.C. and F.P. conceived and designed the experiments. C.C. and G.Y.W. performed the experiments. S.G., G.S.T., H.D.F., C.S., and F.Z. analyzed the data. C.C., C.S., and F.Z. cowrote

the paper. All authors have given approval to the final version of the manuscript.

Funding

This work was supported by National Basic Research Program of China (Grant 2010CB832905) and National Natural Science foundation of China (Grants 51231004 and 51202125).

Notes

The authors declare no competing financial interest.

ABBREVIATIONS

BE, bottom electrode
BRS, bipolar resistive switching
CC, current compliance
CRS, complementary resistive switching
DC, direct current
FFT, fast Fourier transform
fwhm, full width at half-maximum
HRS, high resistance state
LRS, low resistance state
RRAM, resistive random access memory
RT, room temperature
SEM, scanning electron microscopy
TE, top electrode
TEM, transmission electron microscopy
XPS, X-ray photoelectron spectroscopy
XRD, X-ray diffraction

REFERENCES

(1) Terabe, K.; Hasegawa, T.; Nakayama, T.; Aono, M. *Nature* **2005**, *433*, 47−50.
(2) Waser, R.; Aono, M. *Nat. Mater.* **2007**, *6*, 833−840.
(3) Yang, Y. C.; Pan, F.; Liu, Q.; Liu, M.; Zeng, F. *Nano Lett.* **2009**, *9*, 1636−1643.
(4) Pan, F.; Chen, C.; Wang, Z. S.; Yang, Y. C.; Yang, J.; Zeng, F. *Prog. Nat. Sci.* **2010**, *20*, 1−15.
(5) Baek, I. G.; Lee, M. S.; Seo, S.; Lee, M. J.; Seo, D. H.; Suh, D. S.; Park, J. C.; Park, S. O.; Kim, H. S.; Yoo, I. K.; Chung, U. I.; Moon, J. T. In *International Electron Devices Meeting 2004 Technical Digest*; Dec 13−15, 2004 ; IEEE: Piscataway, NJ, 2004; pp 587−590.
(6) Song, S.; Cho, B.; Kim, T. W.; Ji, Y.; Jo, M.; Wang, G.; Choe, M.; Kahng, Y. H.; Hwang, H.; Lee, T. *Adv. Mater.* **2010**, *22*, 5048−5052.
(7) Lee, W.; Park, J.; Kim, S.; Woo, J.; Shin, J.; Choi, G.; Park, S.; Lee, D.; Cha, E.; Lee, B. H.; Hwang, H. *ACS Nano* **2012**, *6*, 8166−8172.
(8) Lee, M. J.; Ahn, S. E.; Lee, C. B.; Kim, C. J.; Jeon, S.; Chung, U. I.; Yoo, I. K.; Park, G. S.; Han, S.; Hwang, I. R.; Park, B. H. *ACS Appl. Mater. Interfaces* **2011**, *3*, 4475−4479.
(9) Kim, G. H.; Lee, J. H.; Jeon, W.; Song, S. J.; Seok, J. Y.; Yoon, J. H.; Yoon, K. J.; Park, T. J.; Hwang, C. S. *ACS Appl. Mater. Interfaces* **2012**, *4*, 5338−5345.
(10) Kim, G. H.; Lee, J. H.; Ahn, Y.; Jeon, W.; Song, S. J.; Seok, J. Y.; Yoon, J. H.; Yoon, K. J.; Park, T. J.; Hwang, C. S. *Adv. Funct. Mater.* **2012**, DOI: 10.1002/adfm.201202170.
(11) Kim, G. H.; Lee, J. H.; Han, J. H.; Song, S. J.; Seok, J. Y.; Yoon, J. H.; Yoon, K. J.; Lee, M. H.; Park, T. J.; Hwang, C. S. *Appl. Phys. Lett.* **2012**, *100*, 213508.
(12) Kim, G. H.; Kim, K. M.; Seok, J. Y.; Lee, H. J.; Cho, D.-Y.; Han, J. H.; Hwang, C. S. *Nanotechnology* **2010**, *21*, 385202.
(13) Linn, E.; Rosezin, R.; Kugeler, C.; Waser, R. *Nat. Mater.* **2010**, *9*, 403−406.
(14) Rosezin, R.; Linn, E.; Nielen, L.; Kugeler, C.; Bruchhaus, R.; Waser, R. *IEEE Electron Device Lett.* **2011**, *32*, 191−193.
(15) Lee, M.-J.; Lee, C. B.; Lee, D.; Lee, S. R.; Chang, M.; Hur, J. H.; Kim, Y.-B.; Kim, C.-J.; Seo, D. H.; Seo, S.; Chung, U. I.; Yoo, I.-K.; Kim, K. *Nat. Mater.* **2011**, *10*, 625−630.
(16) Yang, Y.; Sheridan, P.; Lu, W. *Appl. Phys. Lett.* **2012**, *100*, 203112.
(17) Lee, D.; Park, J.; Jung, S.; Choi, G.; Lee, J.; Kim, S.; Woo, J.; Siddik, M.; Cha, E.; Huang, H. *IEEE Electron Device Lett.* **2012**, *33*, 600−602.
(18) Chai, Y.; Wu, Y.; Takei, K.; Chen, H. Y.; Yu, S. M.; Chan, P. C. H.; Javey, A.; Wong, H. S. P. *IEEE Trans. Electron Devices* **2011**, *58*, 3933−3939.
(19) Yu, S.; Liang, J.; Wu, Y.; Wong, H. S. P. *Nanotechnology* **2010**, *21*, 465202.
(20) Kavehei, O.; Al-Sarawi, S.; Cho, K.-R.; Eshraghian, K.; Abbott, D. *IEEE Trans. Nanotechnol.* **2012**, *11*, 374−385.
(21) Bae, Y. C.; Lee, A. R.; Lee, J. B.; Koo, J. H.; Kwon, K. C.; Park, J. G.; Im, H. S.; Hong, J. P. *Adv. Funct. Mater.* **2012**, *22*, 709−716.
(22) Chen, C.; Yang, Y. C.; Zeng, F.; Pan, F. *Appl. Phys. Lett.* **2010**, *97*, 083502.
(23) Kim, H.-D.; An, H.-M.; Seo, Y.; Kim, T. G. *IEEE Electron Device Lett.* **2011**, *32*, 1125−1127.
(24) Choi, B. J.; Yang, J. J.; Zhang, M. X.; Norris, K. J.; Ohlberg, D. A. A.; Kobayashi, N. P.; Medeiros-Ribeiro, G.; Williams, R. S. *Appl. Phys. A*−*Mater. Sci. Process.* **2012**, *109*, 1−4.
(25) Chen, C.; Gao, S.; Tang, G.; Song, C.; Zeng, F.; Pan, F. *IEEE Electron Device Lett.* **2012**, *33*, 1711−1713.
(26) Chen, C.; Pan, F.; Wang, Z. S.; Zeng, F. *J. Nanosci. Lett.* **2011**, *1*, 102−108.
(27) Kim, H. D.; An, H. M.; Kim, T. G. *IEEE Trans. Electron Devices* **2012**, *59*, 2302−2307.
(28) Rosenberger, L.; Baird, R.; McCullen, E.; Auner, G.; Shreve, G. *Surf. Interface Anal.* **2008**, *40*, 1254−1261.
(29) Barshiha, H. C.; Deepthi, B.; Rajam, K. S. *Thin Solid Films* **2008**, *516*, 4168−4174.
(30) Yang, Y. C.; Gao, P.; Gaba, S.; Chang, T.; Pan, X. Q.; Lu, W. *Nat. Commun.* **2012**, *3*, 732.
(31) Liu, Q.; Long, S. B.; Lv, H. B.; Wang, W.; Niu, J. B.; Huo, Z. L.; Chen, J. N.; Liu, M. *ACS Nano* **2010**, *4*, 6162−6168.
(32) Wang, Z. S.; Zeng, F.; Yang, J.; Chen, C.; Pan, F. *ACS Appl. Mater. Interfaces* **2012**, *4*, 447−453.
(33) Waser, R.; Dittmann, R.; Staikov, G.; Szot, K. *Adv. Mater.* **2009**, *21*, 2632−2663.
(34) Chang, S. H.; Lee, J. S.; Chae, S. C.; Lee, S. B.; Liu, C.; Kahng, B.; Kim, D. W.; Noh, T. W. *Phys. Rev. Lett.* **2009**, *102*, 026801.
(35) Miao, F.; Strachan, J. P.; Yang, J. J.; Zhang, M.-X.; Goldfarb, I.; Torrezan, A. C.; Eschbach, P.; Kelley, R. D.; Medeiros-Ribeiro, G.; Williams, R. S. *Adv. Mater.* **2011**, *23*, 5633−5640.
(36) Chen, M. C.; Chang, T. C.; Tsai, C. T.; Huang, S. Y.; Chen, S. C.; Hu, C. W.; Sze, S. M.; Tsai, M. J. *Appl. Phys. Lett.* **2010**, *96*, 262110.
(37) Guo, X.; Schindler, C. *Appl. Phys. Lett.* **2007**, *91*, 133513.
(38) Chen, G.; Song, C.; Chen, C.; Gao, S.; Zeng, F.; Pan, F. *Adv. Mater.* **2012**, *24*, 3515−3520.
(39) Tseng, H.-C.; Chang, T.-C.; Huang, J.-J.; Yang, P.-C.; Chen, Y.-T.; Jian, F.-Y.; Sze, S. M.; Tsai, M.-J. *Appl. Phys. Lett.* **2011**, *99*, 132104.
(40) Wu, W. T.; Wu, J. J.; Chen, J. S. *ACS Appl. Mater. Interfaces* **2011**, *3*, 2616−2621.
(41) Hassine, N. B.; Mercier, D.; Renaux, P.; Parat, G.; Basrour, S.; Waltz, P.; Chappaz, C.; Ancey, P.; Blonkowski, S. *J. Appl. Phys.* **2009**, *105*, 044111.